Ruthenium Complexes of Quinone Related Ligands: A Study of the Electrochemical Properties of 2-Aminothiophenolatobis(2,2′-Bipyridine)Ruthenium(II)

Mehrdad Ebadi and A. B. P. Lever*

Department of Chemistry, York University, North York, Ontario, Canada, M3J 1P3

Received July 17, 1998

Electrochemical properties of the newly synthesized 2-amino thiophenolatobis(2,2′-bipyridine)ruthenium(II) $[Ru(bpy)_2(NH_2{\cdot}S)cat]^+$ (bpy = 2,2′-bipyridine, $(NH_2{\cdot}S)$ = 2-aminothiophenolate) are reported, using microelectrode, disk electrode, rotating disk electrode cyclic voltammetry, spectroelectrochemistry, and differential pulse voltammetry. The results are compared with the electrochemical properties of the previously studied $[Ru^{II}(bpy)_2LL]^{n+}$ compounds, where LL are 1,2-dihydroxybenzene (O·O), 2-aminophenol ($NH_m{\cdot}O$), and 1,2-diaminobenzene ($NH_m{\cdot}NH_m$). These ligands can exist in protonated ($m = 2$) or deprotonated ($m = 1$) forms. By means of cyclic voltammetry, the deprotonated $[Ru^{II}(bpy)_2(NH{\cdot}S)]^0$ displayed a series of one-electron reversible redox waves, consistent with the previously observed results for the $[Ru^{II}(bpy)_2LL]^{n+}$ complexes. However, the reversible waves observed for protonated $[Ru^{II}(bpy)_2(NH_2{\cdot}S)\ cat]^+$ are inconsistent with the irreversible waves observed for protonated $[Ru^{II}(bpy)_2LL]^{n+}$ complexes. An ECE mechanism is proposed to account for these differences and is used to interpret and simulate the cyclic voltammograms (CV)s of $[Ru^{II}(bpy)_2(NH_2{\cdot}S)cat]^+$ in organic solvents.

1. Introduction

In recent years, there has been a significant interest in the investigation of the redox series of transition-metal complexes involving noninnocent quinone related ligands,[1] of particular interest in the biological field.[2] Many groups,[3−6] including our own,[7−19] have examined the structural characterization, electrochemistry, spectroscopy, magnetic properties, and electronic structure, etc.

(1) Pierpont, C. G.; Lange, C. W. *Prog. Inorg. Chem*. **1994**, *41*, 331.
(2) Guillen, F.; Martinez, M. J.; Munez, C.; Martinez, A. T. *Arch. Biochem. Biophys*. **1997**, *339*, 190. Baez, S.; Sequra-agular, J.; Wildersten, M.; Johansson, A.; Mannervik, B. *Biochem. J*. **1997**, *324*, 25. Fate, R.; Di Bernardo, S.; Estornell, E.; Castelli, G.; Lenaz, G. *Mol. Aspects Med*. **1997**, s269. Muratalie, M.; Klein, M.; Fulco, A.; Feyereisen, R. *Biochemistry* **1997**, *36*, 8401.
(3) Adams, D. M.; Li, B. L.; Simon, J. D.; Hendrickson, D. N. *Angew. Chem., Int. Ed. Engl.* **1995**, *34*, 1481. Ahmed, M.; Khan, Z. H. *Acta Phys. Pol. A* **1995**, *87*, 939. Attia, A. S.; Bhattacharya, S.; Pierpont, C. G. *Inorg. Chem.* **1995**, *34*, 4427. Attia, A. S.; Conklin, B. J.; Lange, C. W.; Pierpont, C. G. *Inorg. Chem.* **1996**, *35*, 1033, 1038. Bhattacharya, S.; Subramanian, M. *J. Chem. Soc., Perkin Trans.* **1996**, 2027; Bodini, M. E.; Arancibia, V. *Trans. Met. Chem.* **1997**, *22*, 150.
(4) Camus, J.; Meghea, A.; Anacona, J. R. *Polyhedron* **1996**, *15*, 2953. Chemerisov, S. D.; Perekhodtsev, G. D.; Tipkin, D. S.; Lebedev, Y. S.; Prokofev, A. I.; Aleksandrov, A. I.; Dubinskii, A. A.; Mobius, K.; Poluektov, O. G.; Schmidt, J. *J. Chem. Soc., Faraday Trans.* **1996**, *92*, 1959. Eduok, E. E.; Krawiec, M.; Buisson, Y. S. L.; OConner, C. J.; Sun, D. L.; Watson, W. H. *J. Chem. Crystallogr.* **1996**, *26*, 621.
(5) Gooden, V. M.; Cai, H. Q.; Dasgupta, T. P.; Gordon, N. R.; Hughes, L. J.; Sadler, G. G. *Inorg. Chim. Acta* **1997**, *255*, 105. Mitra, K. N.; Goswami, S. *Inorg. Chem.* **1997**, *36*, 1322. Handa, M.; Mikuriya, M.; Sato, Y.; Kotera, T.; Nukada, R.; Yoshioka, D.; Kasuga, K. *Bull. Chem. Soc. Jpn.* **1996**, *69*, 3483. Hartl, F. *Inorg. Chim. Acta* **1995**, *232*, 99. Hartl, F.; Vlcek, A. *Inorg. Chem.* **1996**, *35*, 1257. Heinze, F.; Mann, S.; Huttner, G.; Zsolnai, L. *Chem. Ber.* **1996**, *129*, 1115. Heinze, K.; Huttner, G.; Zsolnai, L.; Jacobi, A.; Schober, P. *Chem. A Eur. J.* **1997**, *3*, 732. Hilt, G.; Jarbawi, T.; Heineman, W. R.; Steckhan, E. *Chem. A Eur. J.* **1997**, *3*, 79. Illescas, B.; Martin, N.; Segura, J. L.; Seoane, C.; Orti, E.; Viruela, P. M.; Viruela, R. *J. Org. Chem.* **1995**, *60*, 5643. Jo, D. H.; Jeong, J. H.; Yeo, H. J.; Sohn, Y. S.; Jung, O. S. *Bull. Kor. Chem. Soc.* **1995**, *16*, 504. Jung, O. S.; Jo, D. H.; Lee, Y. A.; Chae, H. K.; Sohn, Y. S. *Bull. Chem. Soc. Jpn.* **1996**, *69*, 2211. Jung, O. S.; Jo, D. H.; Lee, Y. A.; Conklin, B. J.; Pierpont, C. G. *Inorg. Chem.* **1997**, *36*, 19. Jung, O. S.; Jo, D. H.; Lee, Y. A.; Sohn, Y. S.; Pierpont, C. G. *Angew. Chem., Int. Ed. Engl.* **1996**, *35*, 1694.
(6) Keyes, T. E.; Jayaweera, P. M.; McGarvey, J. J.; Vos, J. G. *J. Chem. Soc., Dalton Trans.* **1997**, 1627; Kunzel, A.; Sokolow, M.; Liu, F. Q.; Roesky, H. W.; Noltemeyer, M.; Schmidt, H. G.; Uson, I. *J. Chem. Soc., Dalton Trans.* **1996**, 913; Lyubchenko, S. N.; Kogan, V. A.; Olekhnovich, L. P. *Koord. Khim.* **1996**, *22*, 569. Mcgarvey, B. R.; Ozarowski, A.; Tian, Z. G.; Tuck, D. G. *Can. J. Chem.* **1995**, *73*, 1213. Mishra, L.; Choi, C. S.; Araki, K. *Chem. Lett.* **1997**, 447. Paw, W.; Eisenberg, R. *Inorg. Chem.* **1997**, *36*, 2287. Pierpont, C. G.; Jung, O. S. *Inorg. Chem.* **1995**, *34*, 4281−4283. Roux, C.; Adams, D. M.; Itie, J. P.; Polian, A.; Hendrickson, D. N.; Verdaguer, M. *Inorg. Chem.* **1996**, *35*, 2846. Shirotani, I.; Kudo, T.; Sato, N.; Yamochi, H.; Saito, G. *J. Mater. Chem.* **1995**, *5*, 1357. Simandi, L. I.; Barna, T.; Argay, G.; Simandi, T. L. *Inorg. Chem.* **1995**, *34*, 6337. Speier, G.; Csihony, J.; Whalen, A. M.; Pierpont, C. G. *Inorg. Chim. Acta* **1996**, *245*, 1. Tucker, J. H. R.; Shionoya, M.; Koike, T.; Kimura, E. *Bull. Chem. Soc. Jpn.* **1995**, *68*, 2465. Venkatalakshmi, N.; Rajasekharan, M. V. *Proc. Ind. Acad. Sci. Chem. Sci.* **1995**, *107*, 327. Ward, M. D. *Inorg. Chem.* **1996**, *35*, 1712. Zalis, S.; Fiedler, J.; Pospisil, L.; Fanelli, N.; Lanza, C.; Lampugnani, L. *Microchem. J.* **1996**, *54*, 478.
(7) Haga, M. A.; Dodsworth, E. S.; Lever, A. B. P. *Inorg. Chem.* **1986,** *25*, 447.
(8) Lever, A. B. P.; Auburn, P. R.; Dodsworth, E. S.; Haga, M.; Melnik, M.; Nevin, W. A. *J. Am. Chem. Soc*. **1988,** *110*, 8076.
(9) Auburn, P. R.; Dodsworth, E. S.; Haga, M.; Liu, W.; Nevin, W. A.; Lever, A. B. P. *Inorg. Chem*. **1991**, *31*, 3502.
(10) Masui, H.; Auburn, P. R.; Lever, A. B. P. *Inorg. Chem*. **1991**, *30*, 2402.
(11) Lever, A. B. P.; Masui, H.; Metcalfe, R. A.; Stufkens, D. J.; Dodsworth, E. S.; Auburn, P. R. *Coord. Chem. Rev*. **1993**, *125*, 317.
(12) Masui, H.; Lever, A. B. P.; Dodsworth. E. S. *Inorg. Chem*. **1993**, *32*, 258.
(13) Metcalfe, R. A.; Dodsworth, E. S.; Lever, A. B. P.; Stufkens, D. J.; Pietro, W. J. *Inorg. Chem*. **1993**, *32*, 3581.
(14) Del Medico, A. Dodsworth, E. S.; Auburn, P. R.; Pietro, W. J.; Lever, A. B. P. *Inorg. Chem*. **1994**, *33*, 1583.
(15) Del Medico, A. Dodsworth, E. S.; Auburn, P. R.; Pietro, W. J.; Lever, A. B. P. *Inorg. Chem*. **1995**, *33*, 1507.
(16) da Cunha, C. J.; Fielder, S. S.; Stynes, D. V.; Masui, H.; Auburn, P. R.; Lever, A. B. P. *Inorg. Chim. Acta* **1996**, *242*, 293.
(17) Metcalfe, R. A.; Dodsworth, E. S.; Fielder, S. S.; Stufkens, D. J.; Lever, A. B. P.; Pietro, W. J. *Inorg. Chem*. **1996**, *35*, 7741.

10.1021/ic980838b CCC: $18.00
Published on Web 01/14/1999

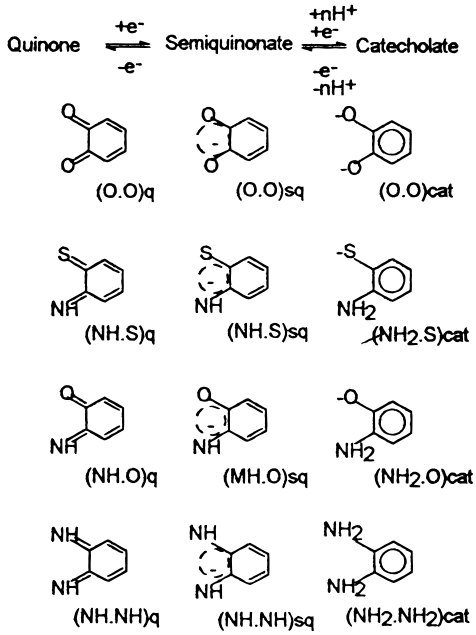

Figure 1. The oxidation states and abbreviations of the orthoquinonoid ligands.

We recently reported[7−12] the electrochemistry of a series of bis(2,2′-bipyridine) ruthenium(II) complexes containing quinonoid ligands, such as catechol (O·O), *o*-aminophenol (NH_m·O), and quinonoiddiamine (NH_m·NH_m) where the coordinating atoms are shown in parentheses. In these complexes the metal center can exist in the Ru^{II} or Ru^{III} oxidation states, the 2,2′-bipyridine (bpy) ligand can be reduced and the quinonoid ligands have three redox forms, the fully reduced catechol ($catH_m$), the partially oxidized semiquinone (sqH_m), and fully oxidized quinone (qH_m) (Figure 1). The subscript *m* reflects the number of protons attached to the donor atoms in each species. The catechol species can, in principle, exist in protonated ($m = 2$), or deprotonated ($m = 1$) forms, with the exception of (O·O) where the coordinated protonated form has not yet been demonstrated in this series of complexes.

In aprotic and very dry solvents, complexes containing the deprotonated quinonoid ligand commonly display two reversible couples corresponding with the q/sq, and sq/cat processes, e.g., q(NH·NH) ↔ sq(NH·NH) ↔ cat(NH·NH). In protic (or wet) solvents, the cat form becomes protonated (but not (O·O)) and these protonated species, such as the $[Ru(bpy)_2(NH_2{\cdot}NH_2)cat]^{2+}$ and $[Ru(bpy)_2(NH_2{\cdot}O)cat]^{+}$ complexes, display two-electron irreversible waves attributed to the loss of protons from the quinonoid nitrogen atoms during the oxidation of the ligand from catechol to the quinone (Figure 2).[10,20]

Electrochemical studies were extended to the Ru(NH_m·S) series to collect comparative data and to evaluate the relevant electrochemical parameters.[21] We had anticipated no new chemistry supposing that the (NH_2·S) system would behave much as the (NH_2·O) system[10] with some shift in potential due to replacement of O by the more electron rich S. However, the (NH_2·S) species did offer new features in its electrochemistry which turned out to be notably solvent dependent. We explore the much richer electrochemical behavior of the $[Ru(bpy)_2(NH_2{\cdot}S)cat]^{+}$ species and compare and contrast the resulting data with earlier data on related systems.

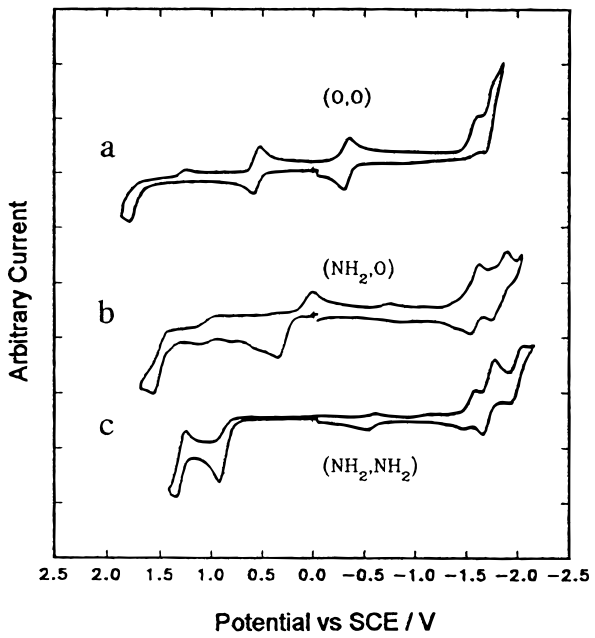

Figure 2. Cyclic voltammograms of (a) $[Ru^{II}(bpy)_2(O{\cdot}O)cat]^0$ in DCE, (b) $[Ru^{II}(bpy)_2(NH_2{\cdot}O)cat]^+$ in DCE. (c) $[Ru^{II}(bpy)_2(NH_2{\cdot}NH_2)cat]^{2+}$ in MeCN. Scan rate 200 mV s^{-1}, 0.1 M $TBAPF_6$, [complex] ~ 10^{-3} M.

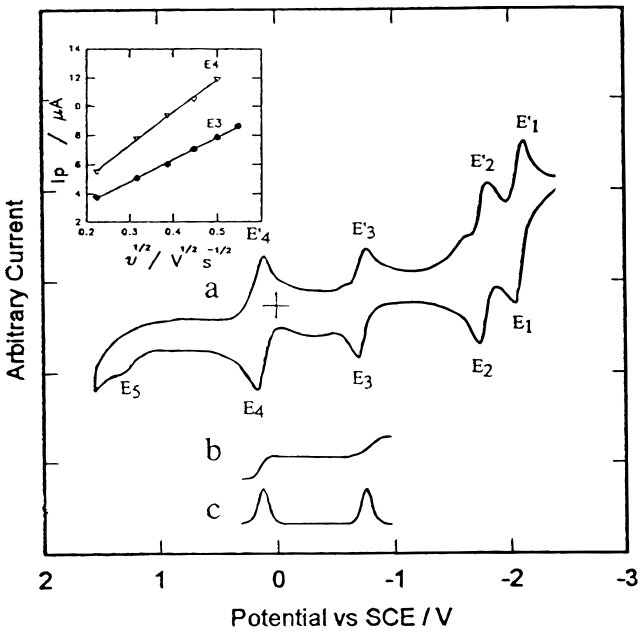

Figure 3. The electrochemistry of $[Ru^{II}(bpy)_2(NH{\cdot}S)sq]^+$ in MeCN, 0.1M $TBAPF_6$, reference vs SCE. (a) Cyclic voltammogram, scan rate 100 mVs^{-1}, (b) microelectrode scan at 1 mVs^{-1}; (c) differential pulse voltammogram scanned toward the negative direction. Pulse width = 40.0 ms, sampling time = 35.0 ms, cycle period = 200 ms, pulse height = 50 mV. (inset) Scan rate dependence of the currents of the E_3 and E_4 waves.

The cyclic voltammograms (CV) generated using $[Ru(bpy)_2(NH{\cdot}S)]^{n+}$ in either the semiquinone or quinone form showed multiple one-electron reversible waves (Figure 3), consistent with the results observed for $[Ru(bpy)_2(NH{\cdot}NH)q]^{2+}$ complexes.[10,12] However, the CV generated using $[Ru^{II}(bpy)_2(NH_2{\cdot}S)cat]^+$ did not show a two-electron irreversible oxidation centered at the (NH_2·S) ligand. Instead, it displayed a variety of CVs in different organic solvents, such as a two-electron

(18) Metcalfe, R. A.; Lever, A. B. P. *Inorg. Chem.* **1997**, *36*, 4762.
(19) DelMedico, A.; Pietro, W. J.; Lever, A. B. P. *Inorg. Chim. Acta*, **1998**, *281*, 126.
(20) Masui, H. Ph.D. Thesis, York University, 1993.
(21) Lever, A. B. P. *Inorg. Chem.* **1990**, *29*, 1271.

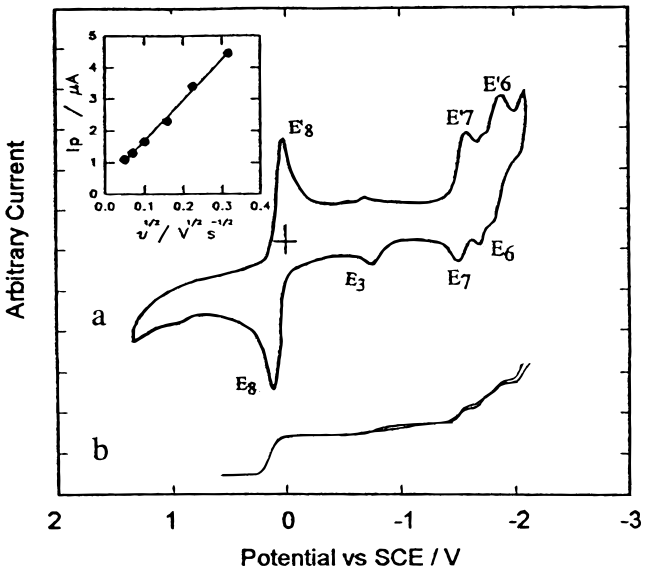

Figure 4. The electrochemistry of $[Ru^{II}(bpy)_2(NH_2{\cdot}S)cat]^+$ in DMF, ca. 3×10^{-3}M, reference vs SCE. (a) Cyclic voltammetry, scan rate 100 mVs^{-1}, 0.1 M $TBAPF_6$, (b) A microelectrode cyclic scan at $1mVs^{-1}$. (Inset) Scan rate dependence of the current of E_8.

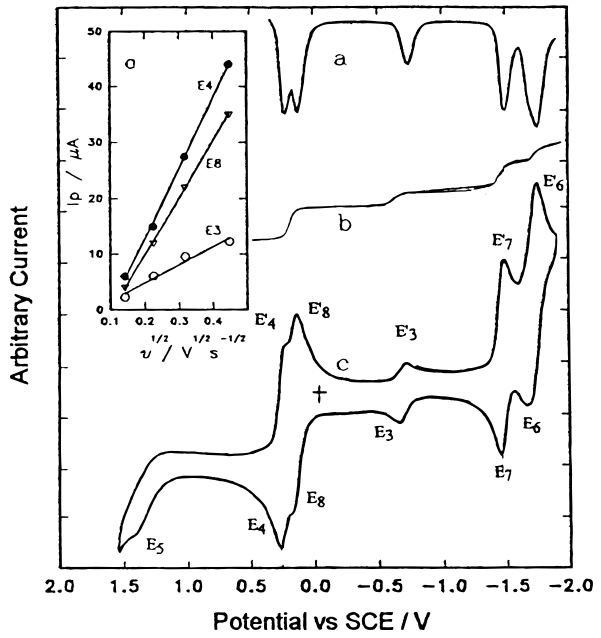

Figure 5. The electrochemistry of $[Ru^{II}(bpy)_2(NH_2{\cdot}S)cat]^+$ in MeCN, 0.1M $TBAPF_6$, ca. 3×10^{-3} M, reference vs SCE. (a) A differential pulse voltammetry scan; scanned toward the negative direction. Pulse width = 40.0 ms, sampling time = 35.0 ms, cycle period = 200 ms, pulse height = 50 mV. (b) A microelectrode cyclic scan at $1mVs^{-1}$; (c) A cyclic voltammogram, scan rate 100 mVs^{-1}, activated Al_2O_3 was added to obtain a very dry solution. (inset) Scan rate dependencies of the CV currents of waves E_3, E_4, and E_8.

reversible wave in dimethylformamide (DMF) (Figure 4), two one-electron reversible waves in acetonitrile (MeCN) (Figure 5), and a one-electron irreversible wave followed by a one-electron reversible wave in pyridine (Py) (Figure 6).

An ECE mechanism is proposed to account for these differences with solvent dependence focused on one particular step. This mechanism is used to explain and simulate the CV of $[Ru^{II}(bpy)_2(NH_2{\cdot}S)cat]^+$ in different organic solvents. It is then examined experimentally using various electrochemical techniques such as microelectrode, spectroelectrochemistry, and differential pulse voltammetry.

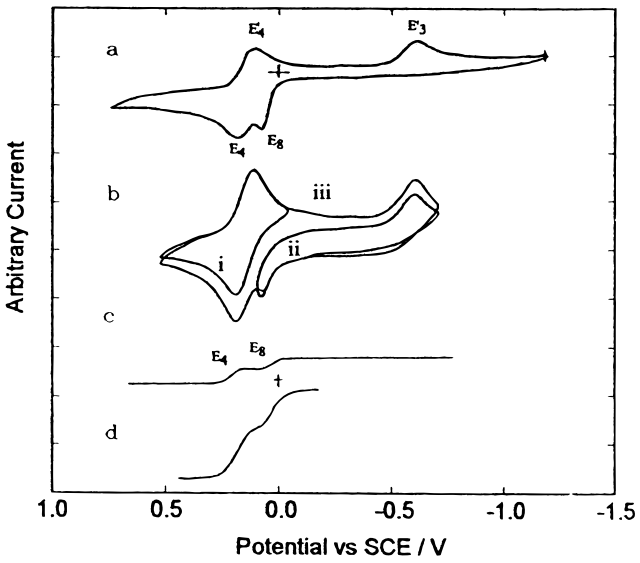

Figure 6. The electrochemistry of $[Ru^{II}(bpy)_2(NH_2{\cdot}S)cat]^+$ ca. 3×10^{-3} M, in pyridine, 0.1 M $TBAPF_6$, reference vs SCE. (a) and (b) cyclic voltammograms with various switching potentials as indicated, scan rate 100 mVs^{-1}. (c) A microelectrode scan at $1mVs^{-1}$; (d) A rotating disk voltammetry scan; scanned toward the positive direction $\omega = 376$ rpm, and scan rate = 4 mV/s.

2. Experimental Section

2.1. Physical Measurement. The electronic spectroscopy measurements were recorded on a Hewlett-Packard 8542A diode array spectrophotometer. Electrochemical data were collected with Princeton Applied Research Corporation model 263 or Cypress system version 5.5 computer controlled electroanalysis system. Cyclic voltammetry was performed in solutions containing 0.1 M $TBAPF_6$, and $(2-3) \times 10^{-3}$ M of the complex. A platinum disk sealed in glass and a platinum wire were used as working and counter electrodes, respectively. AgCl/Ag was used as the quasireference electrode and ferrocene as the internal reference. $Fc^+/Fc = 0.425$ V was assumed in acetonitrile (MeCN), 0.4 V in dimethyl formamide (DMF), and 0.5 V in pyridine (Py) vs SCE.[22] CVs were performed under a nitrogen atmosphere.

Spectroelectrochemistry was performed in a Hartl cell.[23] This cell is equipped with transparent gold foil as the working and the counter electrodes and a AgCl /Ag wire as the reference. Solutions generally contained 0.2 M $TBAPF_6$ and ca. 2×10^{-3} M of the compound under study.

2.2. Chemicals and Solutions. The compounds 2,2′-bipyridyl (99%) and 2-aminothiophenol (99%) were purchased from Aldrich and used without further purification. $Ru(bpy)_2Cl_2$ was synthesized according to literature procedure and further purified by Soxhlet extraction with dichloroethane. NH_4PF_6 (Aldrich) and tetrabutylammonium hexafluorophosphate were recrystallized from methanol. Caledon reagent grade acetonitrile (MeCN) was distilled over P_2O_5, pyridine was distilled over sodium hydroxide (NaOH), followed by partial distillation. Anhydrous grade dimethylformamide (DMF) from Aldrich was used without further purification.

2.3. Preparation of $[Ru(bpy)_2(NH_2{\cdot}S)cat]^+$. Freshly made[24] *cis*-$Ru(bpy)_2Cl_2$ (0.1 g) was added to degassed methanol (30 mL), resulting in a purple solution. The 2-aminothiophenol ligand (0.22 mL) and sodium hydroxide solution (0.1 mL of 0.2 M) were added and the resulting dark brown mixture was refluxed for 18 h. After cooling to

(22) Lever, A. B. P.; Milaeva, E. R.; Speier, G. In *Phthalocyanines: Properties and Applications*; Leznoff, C. C., Lever, A. B. P. Eds.; VCH: New York, 1993; Vol. 3, p 1. Lever, A. B. P.; Wilshire, J. P. *Inorg. Chem.* **1978**, *17*, 1145.
(23) Krejcik, M.; Danek, M.; Hartl, F. *J. Electroanal. Chem.* **1991**, *317*, 179.
(24) Sullivan, B. P.; Salmon, D. J.; Meyer, T. J. *Inorg. Chem.* **1978**, *17*, 3334.

Table 1. Electrochemical Potential Data for Protonated and Unprotonated Species in Organic Solvents[a]

species	solvent	E_5/E'_5	E_4/E'_4	E_8/E'_8	E_3/E'_3	E_7/E'_7	E_6/E'_6	E_2/E'_2	E_1/E'_1
$[Ru(bpy)_2(NH_2{\cdot}NH_2)]^{2+}$	MeCN	1.35	−0.47	0.95[b]	−1.15	−1.48[d]	−1.68[d]	−1.72	−1.82
$[Ru(bpy)_2(NH_2{\cdot}O)cat]^{+e}$	MeCN	1.60[b]	0.1	0.48[b]	−0.75	−1.52[d]	−1.75[d]	−1.66	
$[Ru(bpy)_2(NH_2{\cdot}S)cat]^{+}$	DMF		0.06[c]	0.06[c]	−0.68[d]	−1.55	−1.81[d]		
$[Ru(bpy)_2(NH_2{\cdot}S)cat]^{+}$	MeCN	1.40[b]	0.24	0.15	−0.7	−1.51	−1.74	−1.71	−2.05
$[Ru(bpy)_2(NH_2{\cdot}S)cat]^{+}$	Pc	1.45[b]	0.23	0.15	−0.73	−1.5	−1.73		
$[Ru(bpy)_2(NH_2{\cdot}S)cat]^{+}$	Py		0.15	0.07[b]	−0.62	−1.46			
$[Ru^{II}(bpy)_2(O{\cdot}O)cat]^{0}$	MeCN	1.79[b]	0.56		−0.33			−1.72	

[a] Redox processes are identified in the text. Column 1 identifies the $NH_2{\cdot}X$ species and redox processes involving this protonated species are E_6, E_7, and E_8. All other processes, which are underlined for clarity, involve the deprotonated NH·X species. Data for the $(NH_2{\cdot}NH_2)$, $(NH_2{\cdot}O)$, and (O·O) species are abstracted from ref 10. All the potentials recorded are versus SCE. The potentials were adjusted to SCE using ferrocenium/ferrocene as the internal reference. All processes are chemically reversible except where shown otherwise. However, the E_3/E'_3 process while intrinsically reversible may appear irreversible in some situations depending upon the availability of protons (see text). These data assume Fc^+/Fc at +0.425 V vs SCE in MeCN, +0.4 V in DMF, +0.5 V in Pyridine (Py), and +0.45 V in Propylene carbonate (Pc). [b] Chemically irreversible. [c] Two-electron reversible oxidation (combined E_4, E_8). [d] Quasi-reversible at scan rate of 100 mV/s. [e] Scan rate 200 mV/s.

room temperature, 0.15 mL of NH_4PF_6 solution (0.58 g in 0.6 mL water) was added and the mixture concentrated under a stream of argon over a period of 2 days. During this time, dark purple crystals were deposited from the solution. The crystals were filtered and washed with degassed diethyl ether under a nitrogen environment inside a glovebag. (0.0994 g, 70.8% yield). Anal. Calcd for $C_{26}H_{22}F_6N_5PSRu$: C, 45.75%; H, 3.25%; N, 10.56%. Found: C, 45.44%; H, 3.05%; N, 10.19%. $[Ru(bpy)_2(NH{\cdot}S)sq]^+$ can be prepared from $Ru(bpy)_2(NH_2{\cdot}S)cat]^+$ by treatment of an acetonitrile solution with a few drops of aerated aqueous ammonia, while oxidation of an acetonitrile solution with $AgClO_4$ yields $[Ru(bpy)_2(NH{\cdot}S)q]^{2+}$.

3. Results and Discussions

3.1. Deprotonated Catechol Species. The $[Ru^{II}(bpy)_2(O{\cdot}O)]$ species exhibit multiple one-electron redox couples centered at the metal, quinonoid ligand, and the bipyridine ligands.[7] The assignments are well established.[7−12] Cyclic voltammetric data for $[Ru(bpy)_2(NH{\cdot}O)cat]^+$ and $[Ru(bpy)_2(NH{\cdot}NH)cat]^+$ are similar to those of the (O·O) and (NH·NH) ligand analogues and reported in Table 1 with data illustrated in Figure 2. The same couples and potentials are observed irrespective of the oxidation state of the bulk species (q, sq, or catH).

These assignments were made based on spectroelectrochemistry results. The CV of $[Ru^{II}(bpy)_2(NH{\cdot}S)sq]^+$ in MeCN (Figure 3) resembled that of the $[Ru^{II}(bpy)_2(O{\cdot}O)]^{2+}$ complex,[7] and these waves are assigned accordingly and labeled as noted.

$$[Ru^{II}(bpy^-)(bpy)(NH{\cdot}S)cat]^- + e^- \underset{E'_1}{\overset{E_1}{\rightleftharpoons}} [Ru^{II}(bpy^-)_2(NH{\cdot}S)cat]^{2-} \quad (1)$$

$$[Ru^{II}(bpy)_2(NH{\cdot}S)cat]^0 + e^- \underset{E'_2}{\overset{E_2}{\rightleftharpoons}} [Ru^{II}(bpy^-)(bpy)(NH{\cdot}S)cat]^- \quad (2)$$

$$[Ru^{II}(bpy)_2(NH{\cdot}S)sq]^+ + e^- \underset{E'_3}{\overset{E_3}{\rightleftharpoons}} [Ru^{II}(bpy)_2(NH{\cdot}S)cat]^0 \quad (3)$$

$$[Ru^{II}(bpy)_2(NH{\cdot}S)q]^{2+} + e^- \underset{E'_4}{\overset{E_4}{\rightleftharpoons}} [Ru^{II}(bpy)_2(NH{\cdot}S)sq]^+ \quad (4)$$

$$[Ru^{III}(bpy)_2(NH{\cdot}S)q]^{3+} + e^- \underset{E'_5}{\overset{E_5}{\rightleftharpoons}} [Ru^{II}(bpy)_2(NH{\cdot}S)q]^{2+} \quad (5)$$

The currents for the two E_3/E'_3 and E_4/E'_4 redox couples are shown as a function of scan rate (Figure 3, inset), showing square root dependence. This behavior is characteristic of a diffusion controlled process.[26] The ratio of the anodic to cathodic current in both waves is unity, $I_{p,a}/I_{p,c} = 1$, and is characteristic of a reversible redox reaction.[26] In a reversible, diffusion controlled CV, the number of electrons *n* involved in the redox reaction can be estimated in the redox couple from the peak to peak separation which is 59/n mV. Using the data in Figure 3, *n* values of 1.0 are estimated for both the E_3/E'_3 and E_4/E'_4 redox couples. The differential pulse voltammetry of this solution is shown in Figure 3c. The half-height bandwidth ($W_{1/2}$) can be expressed as[27] $W_{1/2} \approx 90/nF$ (mV) and using data from Figure 3, part c, *n* values of 0.89 and 0.90 were calculated for the E_3/E'_3 and E_4/E'_4 redox couples, consistent with their one-electron nature. Finally, the CV of this system using a microelectrode (Figure 3, part b) demonstrates that the two waves at E_3/E'_3 and E_4/E'_4 have a current height ratio of 1:1. The microelectrode experiment is especially informative since, assuming similar diffusion coefficients for the various redox species, the ratio of peak heights for a pair of redox couples is equal to the ratio of their respective *n* values.[28]

In the following sections the redox waves observed with $[Ru^{II}(bpy)_2(NH_2{\cdot}S)cat]^+$ will be compared to those of the $[Ru^{II}(bpy)_2LL]^{n+}$ species where LL = (O·O), (NH·O), and (NH·NH) (Figure 1).

3.1.1 bpy/bpy$^-$ Redox Waves. The reduction potentials of the bpy ligands in $[Ru^{II}(bpy)_2(NH{\cdot}S)cat]^0$ occur at −1.71 and −2.05 V vs SCE (Table 2) shifted as usual, positively, from the potential for reduction of the free bpy ligand (−2.18 V vs SCE[29]) due to the interaction of the positively charged metal center with the π^* bpy LUMO causing it to be stabilized. The bpy reduction potentials in the $[Ru(bpy)_2LL]^{n+}$ (LL = (NH·S), (NH·O), (NH·NH)) complexes all occur at roughly the same potential. The corresponding reduction potentials for the $[Ru^{II}(bpy)_2(NH_2{\cdot}S)cat]^+$ species lie about 200 mV more positive due to the increased positive charge on the complex (Table 1). We discuss the $Ru^{III/II}$ redox processes below (section 3.3.5).

3.2. Protonated Catecholate Species. The CV of protonated $[Ru^{II}(bpy)_2(NH_2{\cdot}O)cat]^+$ and $[Ru^{II}(bpy)_2(NH_2{\cdot}NH_2)cat]^{2+}$ show a chemically irreversible two-electron oxidation wave.[7] Similar behavior is noted for $[(Ru(NH_3)_4)_2(catH_4{\cdot}catH_4)]^{4+}$ where

(25) Ebadi, M.; Lever, A. B. P. Manuscript in preparation.
(26) Bard, A. J.; Faulkner, L. R. *Electrochemical Methods, Fundamentals and Applications*; John Wiley & Sons: New York, 1980. Gosser, D. K. *Cyclic Voltammetry, Simulation and Analysis of Reaction Mechanisms*; VCH: New York, 1993.
(27) Parry, E. P.; Osteryoung, R. A. *Anal. Chem*, **1964**, *37*, 1634.
(28) Montenegro, M. I.; Queiros, M. A.; Daschbach, J. L. *Microelectrodes, Theory and Applications;* NATO ASI series; Kluwer: Dordrecht, 1991
(29) Kawanishi, Y.; Kitamura, N.; Tazuke, S. *Inorg. Chem*. **1989**, *28*, 2968.

($catH_4$·$catH_4$) is 3,3′,4,4′-tetraaminobiphenyl.[30] This two-electron voltammetry, leading to the [Ru^{II}(q)] species as documented by spectroelectrochemistry,[10,20] is especially well developed in an aqueous acidic solvent such as phosphoric acid. While oxidation of the deprotonated catecholate anion to semiquinone and quinone usually takes place in fully reversible steps in aprotic medium, oxidation of the fully protonated catechol has obviously to involve loss of protons which must occur prior to net oxidation. In an acidic solvent this loss of protons is inhibited.

While amines are usually easy to oxidize, this is not the case if the lone pair is tied up by bonding to a metal center. Thus a coordinated amine is difficult to oxidize. In these systems, the first thermodynamically accessible oxidation is $Ru^{II} \rightarrow Ru^{III}$, at fairly positive potentials, e.g.,

$$[Ru^{III}(bpy)_2(NH_2\cdot S)cat]^{2+} + e^- \leftrightharpoons [Ru^{II}(bpy)_2(NH_2\cdot S)cat]^+ \quad (6)$$

The presence of the Lewis acidic [Ru^{III}] enhances the acidity of the coordinated amine causing loss of protons and this is followed by an internal electronic rearrangement, and oxidation (CE process), namely,

$$[Ru^{III}(bpy)_2(NH_2\cdot S)cat]^{2+} \rightarrow [Ru^{III}(bpy)_2(NH\cdot S)cat]^+ + H^+ \quad (7)$$

$$[Ru^{II}(bpy)_2(NH\cdot S)q]^{2+} + e^- \leftarrow [Ru^{III}(bpy)_2(NH\cdot S)cat]^+ \quad (8)$$

where reaction 8 represents, at a moderately positive potential, a spontaneous loss of the second electron from the [Ru^{III}(NH·S)cat]$^+$ species to yield the final two-electron oxidation product. We were not able to trap the Ru^{III} species to detect its EPR spectrum, but EPR proof of the initial formation of a Ru^{III} species has been presented upon oxidation of an analogous ruthenium(II) complexes of diaminobenzene[20] and 4,5,4′,5′-tetraaminobiphenyl.[30] Presumably [$Ru^{III}(bpy)_2(NH_2\cdot S)cat]^{2+}$ is less stable than the Ru^{III} diamminobenzene derivatives. The chemistry of [$Ru^{II}(bpy)_2(NH_2\cdot S)cat]^+$ in phosphoric acid was studied as a medium which might inhibit the deprotonation step; however, oxidation proceeds at room temperature to the quinone species when a degassed phosphoric solution of the [$Ru^{II}(bpy)_2$-$(NH_2\cdot S)cat]^+$ species is exposed to oxygen.

As outlined in the Introduction, [$Ru^{II}(bpy)_2(NH_2\cdot S)cat$ displayed a variety of CVs in different organic solvents. To assign these redox peaks and the processes involved, the spectroelectrochemistry of the [$Ru^{II}(bpy)_2(NH_2\cdot S)cat]^+$ was explored in the various solvents. The UV assignments to catechol, semiquinone, and the quinone species are based on a detailed study carried out on these complexes using NMR and FTIR spectroscopies, X-ray crystallography, and semiempirical (ZINDO) calculations.[25] The dominant absorption bands in the $Ru^{II}(NH_2\cdot$S) species in the qH, sqH, and $catH_2$ oxidation states lie at 520, 704, and 522 nm, respectively. These bands are used to identify the species but details will be reported elsewhere.[25]

3.3. Mechanisms. The processes occurring in the various solvents are understood in terms of a general set of redox and equilibrium reactions usable for all solvents but where variations in specific equilibrium constants cause the solvent behavior to look quite different. These processes are described by [processes in eqs 3−5 are repeated for clarity]

(30) Metcalfe, R. A.; Vasconcellos, L.; Franco, D. W.; Lever, A. B. P. *J. Chem. Soc., Dalton Trans.* To be submitted.

$$[Ru^{II}(bpy^-)(bpy)(NH_2\cdot S)cat]^0 + e^- \underset{E'_6}{\overset{E_6}{\rightleftharpoons}} [Ru^{II}(bpy^-)_2(NH_2\cdot S)cat]^- \quad (9)$$

$$[Ru^{II}(bpy)_2(NH_2\cdot S)cat]^+ + e^- \underset{E'_7}{\overset{E_7}{\rightleftharpoons}} [Ru^{II}(bpy^-)(bpy)(NH_2\cdot S)cat]^0 \quad (10)$$

$$[Ru^{III}(bpy)_2(NH_2\cdot S)cat]^{2+} + e^- \underset{E'_8}{\overset{E_8}{\rightleftharpoons}} [Ru^{II}(bpy)_2(NH_2\cdot S)cat]^+ \quad (11)$$

$$[Ru^{III}(bpy)_2(NH_2\cdot S)cat]^{2+} \underset{k'_1}{\overset{k_1}{\rightleftharpoons}} [Ru^{II}(bpy)_2(NH\cdot S)sq]^+ + H^+ \quad (12)$$

$$[Ru^{II}(bpy)_2(NH\cdot S)q]^{2+} + e^- \underset{E'_4}{\overset{E_4}{\rightleftharpoons}} [Ru^{II}(bpy)_2(NH\cdot S)sq]^+ \quad (4)$$

$$[Ru^{III}(bpy)_2(NH\cdot S)q]^{3+} + e^- \underset{E'_5}{\overset{E_5}{\rightleftharpoons}} [Ru^{II}(bpy)_2(NH\cdot S)q]^{2+} \quad (5)$$

$$[Ru^{II}(bpy)_2(NH\cdot S)sq]^+ + e^- \underset{E'_3}{\overset{E_3}{\rightleftharpoons}} [Ru^{II}(bpy)_2(NH\cdot S)cat]^0 \quad (3)$$

$$[Ru^{II}(bpy)_2(NH_2\cdot S)cat]^+ \underset{k'_2}{\overset{k_2}{\rightleftharpoons}} [Ru^{II}(bpy)_2(NH\cdot S)cat]^0 + H^+ \quad (13)$$

Each solvent will be discussed in turn with supporting information given below. Processes are labeled consistently so that the same label used for data collected in different solvents reflects the same redox or equilibrium process. The bulk solute species is [$Ru^{II}(bpy)_2(NH_2\cdot S)cat]^+$ in all cases. Under a range of circumstances as defined below, this species is converted to the deprotonated quinone or semiquinone species whose electronic spectra and redox potentials are well defined as described above.

3.3.1. Acetonitrile (MeCN) (Figure 5). The key observations in MeCN solution are controlled potential oxidation just positive of E_4 yields [$Ru^{II}(bpy)_2(NH\cdot S)q]^{2+}$ as deduced by spectroelectrochemistry, while reduction of the solution so generated, at E'_4 yields [$Ru^{II}(bpy)_2(NH\cdot S)sq]^+$ (Figure 7b). In this fashion the E_4/E'_4 couple is identified (eq 4). Reduction of this solution just negative of E'_3 regenerates [$Ru^{II}(bpy)_2(NH_2\cdot S)cat]^+$ Oxidation of this solution at E_8 yields the semiquinone species [$Ru^{II}(bpy)_2(NH\cdot S)sq]^+$ (spectroelectrochemistry, Figure 7a) where a proton is lost relative to the bulk, i.e., processes in eqs 11 and 12.

The data displayed in Figure 8, part a, are very revealing. Using spectroelectrochemistry and beginning positive of E_4, upon scanning negatively, the formation of the semiquinone is followed by plotting the intensity of the semiquinone absorbance at 706 nm, as a function of potential. This absorption band was chosen because it is well separated from the other absorption bands at higher energies. This absorbance is absent with the solution polarized positive of E_4 where the solution is solely in the quinone oxidation state (NH·S)q. At the potential of E'_4, the 706 nm band grows in (see legend for the method of plotting these data) as the semiquinone is formed. At the potential of E'_3, the 706 nm band intensity diminishes as the [$Ru^{II}(bpy)_2$-$(NH\cdot S)cat]^0$ species is formed and then rapidly protonated (λ_{max} 524 nm) (eq 13). This is a Nernstian plot which defines the

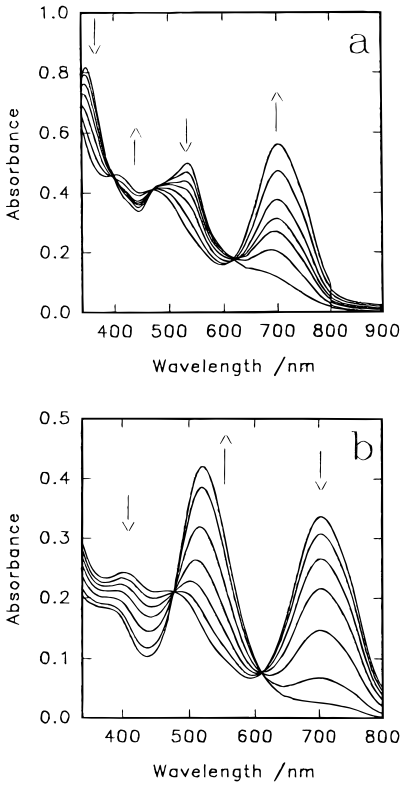

Figure 7. (a) The electronic spectra of $[Ru^{II}(bpy)_2(NH{\cdot}S)sq]^+$ in acetonitrile/0.1 M $TBAPF_6$, as a function of potential the complex is spectroelectrochemically reduced to $[Ru^{II}(bpy)_2(NH_2{\cdot}S)cat]^+$. The semiquinone peak at 704 nm, and protonated catechol peak at 522 nm, distinguish the two species. (b) The electronic spectra of $[Ru^{II}(bpy)_2(NH{\cdot}S)sq]^+$ in acetonitrile/0.1 M $TBAPF_6$, as a function of potential as it is spectroelectrochemically oxidized to $[Ru^{II}(bpy)_2(NH{\cdot}S)q]^{2+}$. The semiquinone peak at 704 nm, and quinone peak at 520 nm, distinguish the two species.

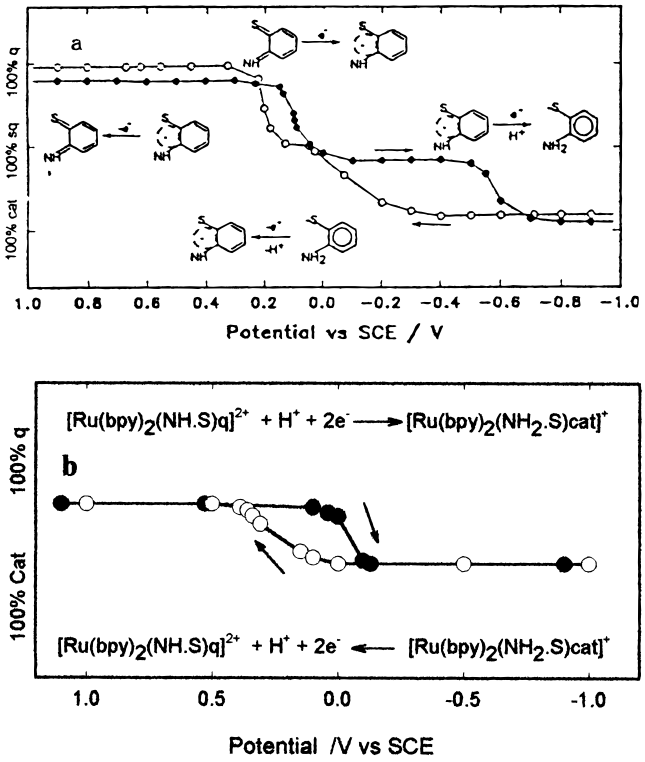

Figure 8. Distribution of various species as a function of potential (Nernstian plot). The intensity of the absorption peak at 706 nm is used to calculate the concentration of each speciesat different potential and applied to the $[Ru(bpy)_2(NH_2{\cdot}S)cat]^+$ species in (a) MeCN and (b) DMF. Solid circles show data scanned from positive to negative potential, while open circles show data scanned from negative to positive potential. The relevant redox reactions observed at each potential, are shown on the diagram. The arrow directions in the structural representations follow the arrow directions in the scan.

potentials for E_3 and E_4 as the midpoints of the sinusoidal curves. Slight variation from the cyclic voltammetric data is probably due to IR drop problems and/or the influence of chemical equilibria.

Continuing with Figure 8, part a, and beginning with bulk $(NH_2{\cdot}S)cat$ at -1.0 V, there is no growth in the 706 nm band until process E_8 is reached where a proton is lost and $(NH{\cdot}S)sq$ is formed. Continuing positive, the semiquinone is soon lost as we move through process E_4 forming the quinone $(NH{\cdot}S)q$ once again.

These data clearly indicate that under steady-state conditions, the processes of net oxidation of the bulk material are

$$[Ru^{II}(bpy)_2(NH_2{\cdot}S)cat]^+ - E_8 \rightarrow [Ru^{II}(bpy)_2(NH{\cdot}S)sq]^+ + H^+ - E_4 \rightarrow [Ru^{II}(bpy)_2(NH{\cdot}S)q]^{2+} \quad (14)$$

while rereduction of the generated $[Ru^{II}(bpy)_2(NH{\cdot}S)q]^{2+}$ proceeds via:

$$[Ru^{II}(bpy)_2(NH{\cdot}S)q]^{2+} - E'_4 \rightarrow [Ru^{II}(bpy)_2(NH{\cdot}S)sq]^+ - E'_3 \rightarrow [Ru^{II}(bpy)_2(NH{\cdot}S)cat]^0 \quad (15)$$

followed rapidly by

$$[Ru^{II}(bpy)_2(NH{\cdot}S)cat]^0 + H^+ \rightarrow [Ru^{II}(bpy)_2(NH_2{\cdot}S)cat]^+ \quad (16)$$

In these experiments, the spectrum of the deprotonated catechol, $[Ru^{II}(bpy)_2(NH{\cdot}S)cat]^0$, has not been observed. It is certainly going to be a very strong base and protonates too rapidly for its spectrum to be identified.

Consider the non-steady-state CV experiment (Figure 5, part c). Beginning at the rest potential (lying between E_3 and E_8,) bulk $[Ru^{II}(bpy)_2(NH_2{\cdot}S)cat]^+$ is oxidized with loss of a proton at E_8 ultimately forming $[Ru^{II}(bpy)_2(NH{\cdot}S)sq]^+$ (eqs 11 and 12) which is then further oxidized at E_4 to $[Ru^{II}(bpy)_2(NH{\cdot}S)q]^{2+}$. E_5 represents an irreversible oxidation to form $[Ru^{III}(bpy)_2(NH{\cdot}S)q]^{3+}$ (see below). Returning, $[Ru^{II}(bpy)_2(NH{\cdot}S)q]^{2+}$ is reduced at E'_4 to regenerate $[Ru^{II}(bpy)_2(NH{\cdot}S)sq]^+$. The protons released in step (eqs 11 and 12)) are still in the vicinity of the electrode. Thermodynamically, the reverse processes (eqs 11 and 12) to regenerate $[Ru^{II}(bpy)_2(NH_2{\cdot}S)cat]^+$ are more favorable than reduction of $[Ru^{II}(bpy)_2(NH{\cdot}S)sq]^+$ to $[Ru^{II}(bpy)_2(NH{\cdot}S)cat]^0$. Thus the CV experiment indicates that most of the $[Ru^{II}(bpy)_2(NH{\cdot}S)sq]^+$ is reduced at E'_8 to form $[Ru^{II}(bpy)_2(NH_2{\cdot}S)cat]^+$. The presence of the low current wave at E'_3/E_3 shows that some equilibrium amount of $[Ru^{II}(bpy)_2(NH{\cdot}S)sq]^+$ generated at E'_4 remains un-protonated and is reduced to $[Ru^{II}(bpy)_2(NH{\cdot}S)cat]^0$ at E'_3 [see simulation in section 3.4].

Steady-state data are shown in the microelectrode study (Figure 5, part b). The wave near 0 V comprises both the E_8 and E_4 processes. The total current (two-electrons) of E_6 and E_7, representing the two successive reductions of the bipyridine ring, is equal to the sum of the currents at E_8, E_4, and E_3. Simulation (see section 3.4) of the rotating disk electrode study also reproduces the scan in Figure 5, part b. Note that the very

small current at E_3 is a consequence of starting the microelectrode scan at a potential positive of E_4. At this potential, some $[Ru^{II}(bpy)_2(NH{\cdot}S)q]^{2+}$ is formed in the vicinity of the electrode, is reduced at E_4 to $[Ru^{II}(bpy)_2(NH{\cdot}S)sq]^{+}$ and, as noted above, some of this remains to be reduced at E_3. There is no wave observed at E_3 if the scan is begun from a potential negative of E_3. If an organic acid, such as trifluoracetic acid is added to the solvent, the waves at E'_3/E_3 are totally absent from all voltammograms since equilibrium (eq 13) will now lie totally to the left.

Processes E'_6/E_6 and E'_7/E_7 are the successive reductions of the bipyridine ligands bound to the protonated $[Ru^{II}(bpy)_2(NH_2{\cdot}S)cat]^{+}$ species occurring some 200 mV more positive than for $[Ru^{II}(bpy)_2(NH{\cdot}S)cat]^{0}$ because of the extra positive charge on the complex. This experiment has been digitally simulated (see section 3.4).

3.3.2. Dimethylformamide (DMF) (Data in Figure 4). The data in DMF are readily understood on the basis of the previous discussion, In this solvent the two waves E'_4/E_4 and E'_8/E_8 have coalesced into one two-electron process which shows just a very minimal amount of separation into two components. Spectroelectrochemistry through that region does generate a small amount of semiquinone but it is transient and otherwise shows the two-electron interconversion between $[Ru^{II}(bpy)_2(NH_2{\cdot}S)cat]^{+}$ and $[Ru^{II}(bpy)_2(NH{\cdot}S)q]^{2+}$. The Nernstian graph of concentration ratio versus potential (Figure 8, part b) shows some separation between the two processes (eqs 4, 11, and 12).

3.3.3. Pyridine (Py) (Data in Figure 6). The cyclic voltammogram of $[Ru^{II}(bpy)_2(NH_2{\cdot}S)cat]^{+}$ in pyridine displays a reversible wave at E_4/E'_4, and two irreversible waves at E_8 and E'_3 potentials (Figure 6). The wave at E'_3 is coupled to E_8 as in MeCN, but in this case there is no wave E'_8 nor E_3. Wave E_8 is absent when cycling around E_4/E'_4 (Figure 6, part b, curve i) but reappears if the negative going sweep is extended to include E'_3 (Figure 6, part b, curve iii). Thus the irreversible wave at E'_3 is the reverse process of the wave at E_8.

While the CV looks very different from that in MeCN and DMF, the interpretation is straightforward with one crucial difference. Oxidation of $[Ru^{II}(bpy)_2(NH_2{\cdot}S)cat]^{+}$ at E_8 results in deprotonation and formation of $[Ru^{II}(bpy)_2(NH{\cdot}S)sq]^{+}$ and this is followed at E_4 by formation of $[Ru^{II}(bpy)_2(NH{\cdot}S)q]^{2+}$ The semiquinone is reformed at E'_4, but in pyridine the released protons are tied up by the very basic pyridine and the semiquinone is unable to extract them to regenerate $[Ru^{III}(bpy)_2(NH_2{\cdot}S)cat]^{2+}$ directly. Thus all of the $[Ru^{II}(bpy)_2(NH{\cdot}S)sq]^{+}$ formed at E'_4 is reduced at E'_3 where the $[Ru^{II}(bpy)_2(NH{\cdot}S)cat]^{0}$ generated is evidently a strong enough base to remove the extant protons from pyridine (absence of return wave E_3). The microelectrode and rotating disk data (Figure 6, part d) confirm the 1:1 nature of the current flow at E_8 and E_4.

To test the hypotheses, a small amount of concentrated NH_3 was added during the CV in MeCN. The reversible wave at E_8/E'_8 became totally irreversible and the CV resembled that generated in pyridine, confirming the hypothesis. The CV and microelectrode/RDE behavior in pyridine have also been simulated (section 3.4).

3.3.4. Quinonoid Ligand Redox Waves (E_3, E_4). In these $[Ru(bpy)_2LL]^{n+}$complexes, the potentials for the reversible oxidation (E_3,E_4) of the quinonoid ligands (in their sqH or catH forms) shift significantly toward more negative values by replacing the oxygen atoms with the more electron rich nitrogen atoms in the quinonoid ligand (Table 1). Replacing oxygen with the more electron rich sulfur has a very much smaller effect.

3.3.5. Ru^{III}/Ru^{II} Redox Processes and $E_L(L)$ Parameters (E_5, E_8). The E_5 processes tend to be irreversible and hence represent a minimum value for the $Ru^{III/II}[NH{\cdot}X]q$ couple. The E_8 processes, corresponding with the $Ru^{III/II}[NH_2{\cdot}X]cat$ couple, can appear reversible but are followed by rapid loss of protons. For this latter couple there is a distinct difference between the various species with the $Ru^{III/II}$ couple shifting to more positive values in the sequence $X = S < O < NH_2{\cdot}$ In this case, then, replacement of oxygen by the more electron rich sulfur does have a significant effect in making the ruthenium easier to oxidize. This can be understood by recognizing that in these catecholate species the extra electron density remains localized on sulfur since the charge cannot delocalize onto the ring to any significant degree; it can therefore influence the $Ru^{III/II}$ potential. However, there is literature evidence[31,32] for metal based redox couples such as $Mo^{V/IV}$ showing the reverse sequence with the oxygen based ligand causing the metal to be much easier to oxidize than the analogous sulfur ligand. This has been discussed in some depth.[32]

With respect to the q/sq and sq/cat redox processes discussed above, the extra charge can delocalize into the ring in the q and sq oxidation states, so that the effect of replacing O by S is muted. With $X = NH_2$ there is an extra positive charge on the species accounting for the more positive oxidation potential.

Knowledge of the $Ru^{III/II}$ potential could, in principle, lead to evaluation of the magnitude of the $E_L(L)$ parameter[21] which is a measure of the donor and acceptor characteristics of the ligand.[33] Knowledge of the comparative $E_L(L)$ values for these ligands would then be useful to have, especially as a function of the oxidation state of the quinonoid ligand. However, given that the $Ru^{III/II}$ data are not fully reversible and any $E_L(L)$ values would only reflect a single datum, and hence not statistically very useful, we do not try to extract $E_L(L)$ values for these ligands at the present time.

3.4. Simulation of the Cyclic Voltammograms. To examine the redox mechanism illustrated by the cyclic voltammetry in pyridine and MeCN, these data were simulated using the Digisim[8] program version 2.1 (Bioanalytical Systems, Inc.). The potentials for the various redox processes are those portrayed in Table 1. Equilibrium and rate constants required for eqs 12 and 13 were varied to obtain a reasonable fit to the response. However, no attempt was made to achieve a perfect fit since to be useful this would require a very much more detailed statistical analysis of the experimental data, and this was not obtained. The resulting equilibrium and rate constants, shown in the legend, should then be considered as illustrative but not definitive.

Figure 9 displays the simulated CV and RDE data for $[Ru^{II}(bpy)_2(NH_2{\cdot}S)cat]^{+}$ in MeCN, and these closely resemble the experimental data shown in Figure 5.

To simulate the CV of $[Ru^{II}(bpy)_2(NH_2{\cdot}S)cat]^{+}$ in pyridine, an additional homogeneous chemical reaction was added to present the basic nature of the solution

$$B + H^{+} \leftrightharpoons BH^{+} \qquad (17)$$

Figure 10 displays the simulated CV and RDE data for $[Ru^{II}(bpy)_2(NH_2{\cdot}S)cat]^{+}$ in pyridine, again closely resembling

(31) Cleland, W. E., Jr.; Barnhart, K. M.; Yamanouchi, K.; Collison, D.; Mabbs, F. E.; Ortega, R. B.; Enemark, J. M. *Inorg. Chem.* **1987**, *26*, 1017.
(32) Olson, G. M.; Schultz, F. A. *Inorg. Chim. Acta* **1994**, *225*, 1.
(33) Fielder, S. S.; Osborne, M. C.; Lever, A. B. P.; Pietro, W. J. *J. Am. Chem. Soc.* **1995**, *117*, 6990.

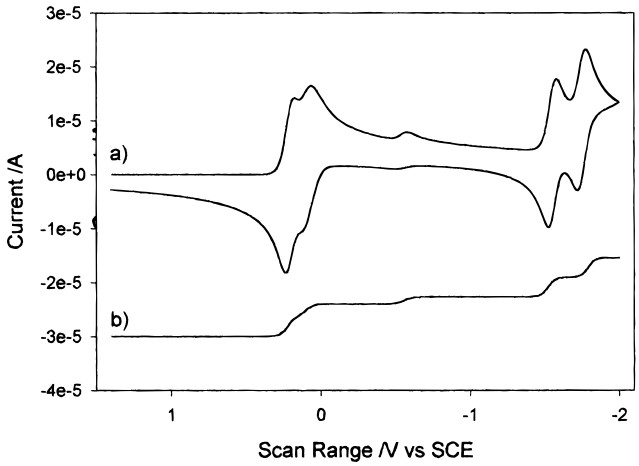

Figure 9. Digisim[8] simulation of the acetonitrile data shown in Figure 5. See text section 3.4 for details. Simulation mechanism involves eqs 3, 4, and 9−13. Potentials are those shown in Table 1. For eq 12 K = 0.01, $k_1 = 1 \times 10^4$, $k_1' = 1 \times 10^6$. For eq 13, $K = 4.3 \times 10^{-17}$ (a) cyclic voltammogram, 100 mVs^{-1}; (b) rotating disk electrode voltammogram (steady state, will mimic microelectrode study). The current has been scaled to place both sets of data together for comparison.

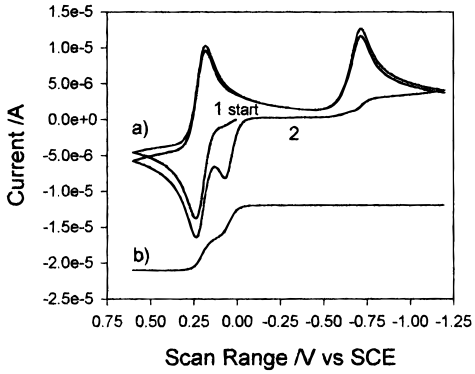

Figure 10. Digisim[8] simulation of the pyridine data shown in Figure 6. See text section 3.4 for details. Simulation mechanism involves eqs 3, 4, 11−13, and 17. Potentials are those shown in Table 1. For eq 12, $K = 0.01$, $k_1 = 1 \times 10^4$, $k_1' = 1 \times 10^6$. For eq 13, $K = 4.3 \times 10^{-17}$, $k_2 = 4.3 \times 10^{-7}$, $k_2' = 1 \times 10^{10}$. For eq 17, $K = 1 \times 10^7$, $k_f = 1 \times 10^7$, $k_b = 1$. (a) Cyclic voltammogram, 100 mVs^{-1}; (b) rotating disk electrode voltammogram (steady state, will mimic microelectrode study). The current has been scaled to place both sets of data together for comparison.

the experimental data shown in Figure 6. Both experimental CVs in MeCN and pyridine were simulated by using the proposed mechanism, and the conversion of one simulated CV to another by addition of eq 17 to the mechanism, is consistent with the experimental result where addition of base to MeCN would generate a CV resembling that one in pyridine. Further, the simulated voltammetry used the same equilibrium constant and rate constant data for eq 12 in both solvents, with a small equilibrium constant indicating that equilibrium eq 12 is rather finely poised and hence the relative concentrations of the species are easily influenced by solvent acidity and basicity. The equilibrium constant for eq 13 is determined by thermodynamics of the system, by the value of K chosen for eq 12 and the observed redox potentials. It is very small, the equilibrium lying strongly to the left as expected. There is therefore only one equilibrium constant to fit.

4. Conclusions

The mechanisms described in eqs 3−18 can account for the various differences observed for the electrochemical behavior of the $[Ru(bpy)_2(NH_2{\cdot}S)catH_2]^{2+}$ species in various solvents. The rather remarkable differences arise from relatively small changes in protonation equilibria influenced by the basicity or lack of basicity of the solvent. The addition of ammonia to a nonbasic solvent or of an acid such as trifluoracetic acid to a basic solvent cause changes which mimic the solvent variations. Microelectrode and rotating disk studies, and digital simulation analyses provide additional confirmatory evidence for the validity of the treatment.

Consideration of the data in Table 1 reveals that while there are marked differences in potentials between $NH_m{\cdot}X$ (X = NH, O), data for X = O and S are rather similar. The key observation is that for X = S, $E_8 < E_4$ while for X = NH, O, $E_8 > E_4$. In the former situation E_8 and E_4 appear as two independent one-electron processes, albeit coincident in DMF solution. When E_8 lies above E_4 in potential, oxidation of $[Ru^{II}(NH_2{\cdot}X)cat]^{n+}$ leads to $[Ru^{III}(NH_2{\cdot}X)cat]^{(n+1)+}$, which loses a proton and rearranges to $[Ru^{II}(NH{\cdot}X)sq]^{n+}$, but this species is now lying at a potential greater than E_4 so it immediately oxidizes to $[Ru^{II}(NH{\cdot}X)q]^{(n+1)+}$, thus the process at E_8 appears as a two-electron oxidation.

The parameters arising from the simulations cannot be assumed statistically accurate but they do show that eq 12 is finely poised, and eq 13 lies strongly to the left. Thus the mechanism proposed to account for the unusual solvent behavior is confirmed.

Acknowledgment. We thank the Natural Science and Engineering Research Council (Ottawa) for financial support. We also thank Johnson Matthey, Inc., for the loan of ruthenium trichloride, Dr. Elaine S. Dodsworth for valuable discussion, Dr. Pamela R. Auburn for the initial synthesis of the (NH·S)q species, and Ms Lori Payne for some preliminary experiments.

IC980838B